J. Fluid Mech. (2008), *vol.* 602, *pp.* 219–239.
doi:10.1017/S0022112008000839 Printed in the United Kingdom

Interleaving intrusions produced by internal waves: a laboratory experiment

ROSS W. GRIFFITHS[1] AND ALI A. BIDOKHTI[2]

[1]Research School of Earth Sciences, Australian National University, Canberra, ACT 0200, Australia

[2]Institute of Geophysics, Tehran University, Tehran, PO Box 14155-6466, Iran

(Received 24 March 2006 and in revised form 25 January 2008)

A statically stable stratified water column that also contains horizontal property contrasts (either of passive tracer alone or of two dynamically active solutes) is generated and continuously maintained for a long period by releasing two turbulent buoyant plumes of equal buoyancy fluxes into opposite ends of a long channel of water. The bottom outflows from the plumes also continuously excite internal gravity waves that produce a series of counter-flowing quasi-horizontal shear layers which are quasi-stationary relative to the box but whose phase propagates downward through the upward-moving water column. We report that the flow further involves an oscillation associated with the internal waves that gives rise to a sequence of interleaving intrusions across the horizontal gradient region. The wave-driven intrusions are advected upward with the 'filling-box' circulation and have the appearance of a spatially growing instability. The intrusions are examined in cases having no horizontal property differences other than a passive tracer. In further experiments where one plume is salt solution and the other is sugar solution, there is vigorous double-diffusive convection on the interleaving intrusions, including salt fingering and diffusive density interfaces, but this convection has only a weak influence on the intrusion thicknesses and velocities. We conclude that under all conditions attained in these experiments, the interleaving is driven by internal waves and not by the property gradients, and we infer that the wave-generated intrusions enhance double-diffusive buoyancy fluxes.

1. Introduction

The formation of multiple horizontal intrusions and convecting layers due to the instability of horizontal property or density differences in a stratified fluid has been examined in many experiments with double-diffusive convection. These include experiments with sidewall heating or cooling of a salinity gradient (Thorpe, Hutt & Soulsby 1969; Hart 1973; Chen 1974; Narusawa & Suzukawa 1981; Tanny & Tsinober 1988; Jeevaraj & Imberger 1991; Chen & Chen 1997; Malki-Epshtein, Phillips & Huppert 2004), and the melting of a vertical ice interface in a salinity gradient (Huppert & Turner 1980; Josberger & Martin 1981). They also include experiments with the instability of a vertical interface (or density compensated front) between waters initially having different composition but no horizontal density difference and the same vertical density gradient (Ruddick & Turner 1979; Ruddick, Phillips & Turner 1999). The latter case is reviewed by Ruddick (2003). Similar double-diffusive intrusions and multi-layered flow can occur when a solution of one composition is released at its neutral buoyancy level in a gradient of another property (e.g. saltwater into aqueous sugar solution) (Turner 1978; Turner & Chen 1974;

Nagasaka, Nagashima & Yoshida 1995). In all of these cases, interleaving intrusions and subsequent layering is attributed to the growth of an instability that relies on the differential molecular diffusion of heat and solute or of two solutes. Multiple buoyancy-driven intrusions can also be formed as a result of localized turbulent mixing, in which case the vertically mixed fluid can collapse into the surrounding density gradient as many horizontal tongues (Browand, Guyomar & Yoon 1987).

One important application of the above laboratory studies and related theoretical analyses is to understand the extensive occurrences of interleaving intrusions in the oceans. However, as discussed by Ruddick & Richards (2003), there is still no clear picture of their formation mechanism and, in particular, the degree to which oceanic interleaving is a result of double-diffusive processes. Here we report experiments in which another mechanism – low-frequency travelling internal waves (or shear modes) – produce intrusions in a region of horizontal property gradients. We also investigate the superposed effects of the shear modes and double-diffusive convection. The study relies on a simple method of creating and continuously maintaining a density-compensated region of horizontal gradient, referred to in oceanography as a 'front'.

No significant role of internal waves in forming interleaving intrusions has been reported, in either the laboratory or the oceans. In the oceans there is a ubiquitous presence of internal inertial–gravity waves (Garrett & Munk 1972, 1979) having an energy spectrum dominated by low (near-inertial) frequencies. The resulting quasi-horizontal wave displacements have the potential to produce interleaving of water properties at length and time scales determined by the dominant wavelengths present (Fedorov 1978; Georgi 1978), and the horizontal velocities involved would typically be large compared with the velocities that could be driven by double-diffusive convection. Such interleaving would enhance vertical property gradients, as well as increasing the contact area between waters of differing properties, potentially stimulating parasitic double-diffusive convection and increasing buoyancy fluxes. We also conjecture that under suitable conditions the buoyancy fluxes might take over the driving role for the interleaving when intrusions reach large amplitude. A contrary view is that the (nearly reversible) displacements of travelling internal waves are of too short a period to give rise to intrusions of the large horizontal extent observed in the oceans.

In previous laboratory experiments with interleaving the horizontal growth of intrusions was governed by an applied horizontal difference (e.g. a horizontal concentration difference ΔS across the front or a sidewall temperature difference) and driven by a vertical divergence of the double-diffusive buoyancy flux between layers. For example, in the classic 'dam-break' double-diffusive front experiments of Ruddick & Turner (1979) (where NaCl and sugar were used to model heat and salt) the vertical scale of the initial instability (and the subsequent thickness of the layers) was proportional to $D^* = g\beta\Delta S/N^2$, where g is the gravitational acceleration, $\beta\Delta S$ would be the horizontal density difference due to the concentration difference ΔS if this one component alone were present, and N is the pre-existing buoyancy frequency. The rate of lateral extension of the intrusions was proportional to ND^* (Ruddick & Turner 1979; Ruddick *et al.* 1999; Malki-Epshtein *et al.* 2004). The interleaving layers were broad shallow convection cells driven by the vertical double-diffusive buoyancy fluxes between layers. As a consequence, the intrusions sloped across isopycnals and geopotential surfaces.

The initial instability in all of these experiments shows no dependence on the finite length of the box, and was therefore not apparently influenced by internal wave normal modes excited by the instability. Malki-Epshtein *et al.* (2004) and Browand *et al.* (1987), observing double-diffusive instability and the collapse of a turbulent front,

respectively, report that the growing intrusions excited the zero-frequency (horizontal columnar) internal wave modes having a vertical wavelength comparable to that of the initial convective instability. This led to a dependence of the intrusion speed on the tank length. The stratified environment far from the forcing sidewall or front was set into motion by these columnar modes and modified toward a staircase structure on a time scale set by the internal wave travel time along the box. In the double-diffusive case the stratification is altered first by the columnar modes and later by the arrival of the convecting intrusion. In all of the cases mentioned so far, the internal modes have zero vertical phase velocity and are produced by the intrusions themselves. However, for the case of a small localized salt source in a sugar gradient Nagasaka *et al.* (1995) speculated that the vertical scale of the multiple double-diffusive intrusions observed might be established by internal waves.

In order to examine the interactions of travelling (non-zero-frequency) internal waves with a 'front' it is necessary to identify a means of continuously maintaining in the laboratory a horizontal property gradient in a stratified environment and, at the same time, create internal wave disturbances. A solution was found in a modification of the experiments of Wong, Griffiths & Hughes (2001, hereinafter referred to as WGH01). Their experiments showed that a turbulent plume of salt solution falling into a long channel of initially fresh water generates not only the well-known filling-box density stratification of Baines & Turner (1969), but also strong horizontal shearing layers. Theoretical solutions given by WGH01 (for the two cases of inviscid waves in the nonlinear filling-box density profile and viscous waves in a stratification of uniform buoyancy frequency) showed that the plume outflow along the base excites a dominant wave mode that carries energy and momentum upward from the level of the plume outflow at the base. The mode has a downward phase speed equal and opposite to the slow vertical advection speed of the filling-box circulation. Thus the dominant mode, excited because it is stationary relative to the tank, propagates downward through the water. It was also shown that these waves govern the thickness of the plume outflow, and that the wave dynamics imply a characteristic Froude number for the outflow. Waves of higher frequency play no obvious role, and in laboratory experiments the turbulence in the plume has frequencies higher than the buoyancy frequency in the surrounding gradient.

The experiments of WGH01 used a single component and therefore involved no double-diffusive convection. Similar shear layers were utilized by Wells, Griffiths & Turner (2001) to examine the formation of layered fine structure through the interaction of salt-fingering convection with shear. In that case, the shear was excited by inflow of solution at one corner of a box which slowly filled the box with superposed vertical gradients of salt and sugar in the sense favourable to salt fingering. The arrangement produced horizontal flow at the level of the input (somewhat similar to the plume outflow in WGH01) and shear layers throughout the depth. We infer that the vertical wavelength was set by internal wave motions which had a vertical phase speed (relative to the fluid) equal to the rate at which the source moved upward as the water depth increased. Salt-fingering convection was vigorous and led to modification of the local density structure in each layer.

In the laboratory experiments reported here, we use two turbulent plumes in order to generate a horizontal gradient of passive tracer or composition, but not of density. The aim is to continuously maintain in a quasi-steady state a horizontal gradient, generate travelling internal wave modes, and observe the interaction of the two. The horizontal gradient in this case occurs across a sharp vertical interface near the base and this evolves with height, owing to horizontal transport by intrusions,

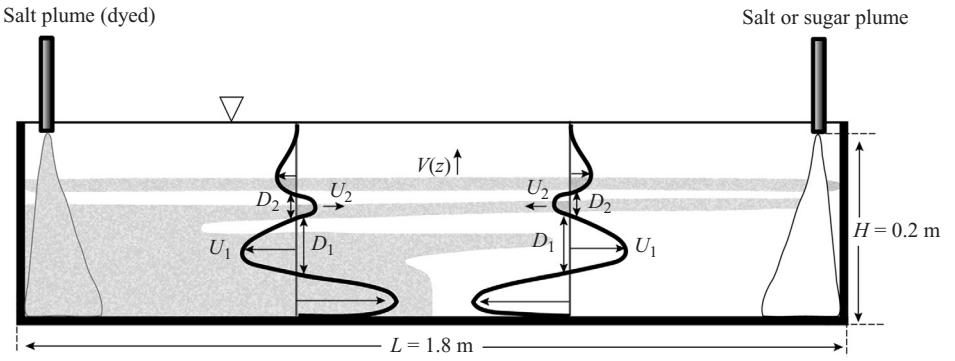

FIGURE 1. Diagrammatic sketch of the flow and definitions of the measured flow variables. Shearing layers are indicated by vertical profiles of horizontal velocity, roughly symmetric about the centre of the channel. Compositional layers, as shown by passive tracer, are shown in grey scale. This is a snapshot in time as each compositional layer moves upward through the shear layers and becomes thinner. Above the level of the first shear layer there is no correlation between the velocity layers and compositional layers.

to become a broad horizontal gradient at higher levels in the tank (which can be thought of as downstream in the filling-box circulation). A notable aspect is that the horizontal gradient is continuously maintained. These aspects contrast with the temporally evolving interleaving front created by the initial removal of a vertical barrier (Ruddick & Turner 1979). Another difference is that the sustained internal wave activity is not generated by the intrusions. Many aspects of the flow have been explored previously. Here we focus on novel aspects associated with having two plumes instead of one. In § 3 we report qualitative observations of the formation of interleaving intrusions and in § 4 we discuss the horizontal velocities and vertical length scales of the intrusions.

2. The experiments

Most of the experiments were carried out in a glass tank 1.8 m long, 0.15 m wide and 0.3 m deep. The tank was initially filled to a depth of 0.22 m with fresh water. Two negatively buoyant turbulent plumes were fed from vertical tubes of 3 mm inner diameter placed at equal distances from the side and end walls of the tank and at 0.2 m or 0.1 m from the bottom of the tank (figure 1). A multi-head mini peristaltic pump supplied, within measurement uncertainties, constant and equal volume fluxes Q of aqueous salt or sugar solutions to these tubes (except in a few runs where temperature and salinity differences were used). The two solutions usually had equal density differences $\Delta\rho$ from freshwater (the initial tank fluid). Hence the two plume sources in most runs had equal buoyancy fluxes $F = g\Delta\rho Q$, where g is the gravitational acceleration. The temperature of the water was constant to within 1° C throughout each run and also within 1° C of room temperature.

The plumes generated the 'filling-box' density profile of Baines & Turner (1969). We also observed that, up to the effect of interleaving across the front, each plume tended to supply the adjacent half of the tank such that the box-scale circulation consisted of two cells and was nearly symmetric about the mid-point of the channel. The turbulent plumes were axisymmetric and flow in the vicinity of the plumes was three dimensional, as assumed in the Baines & Turner (1969) theory. However, the channel length was chosen large enough such that flow in most of its length was

Run	Q (ml min^{-1})	$F \times 10^7$ (m^4 s^{-3}) ($\pm$0.01)	P (s) ($\pm$20)	D_1 (mm) ($\pm$1.0)	D_2 (mm) ($\pm$1.0)	U_1 (mm s^{-1}) ($\pm$0.05)	U_2 (mm s^{-1}) ($\pm$0.05)	V (mm s^{-1}) ($\pm$0.02)	Type
1	5	0.32	500	29.0	25.0	1.10	0.14	0.054	Salt
2	5	0.32	700	32.5	27.0	0.95	0.16	0.060	Salt-sug
3	5	0.56	280	30.4	25.0	1.40	0.21	0.040	Salt
4	5	0.56	240	29.5	26.0	1.25	0.22	0.078	Salt-sug
5	5	0.74	360	26.0	23.0	1.70	0.16	0.046	Salt
6	5	0.74	420	28.0	26.0	1.40	0.21	0.063	Salt-sug
7	5	1.13	145	31.0	22.0	2.10	0.23	0.058	Salt
8	5	1.13	240	33.0	26.5	1.70	0.26	0.040	Salt-sug
9	5	1.88	208	30.0	26.0	2.65	0.26	0.060	Salt
10	5	1.48	190	32.0	31.0	2.10	0.35	0.050	Salt-sug
11	5	1.92	120	28.0	28.0	3.10	0.36	0.104	Salt
12	5	1.92	200	32.0	31.5	2.50	0.55	0.110	Salt-sug
13	5	2.51	100	29.0	28.0	3.50	0.47	0.110	Salt
14	5	2.51	110	32.8	31.0	2.70	0.57	0.085	Salt-sug
15	5	2.93	130	35.4	28.0	3.95	0.54	0.087	Salt
16	5	2.93	150	37.5	32.0	2.80	0.52	0.110	Salt-sug
17	14	4.13	120	33.5	28.0	4.70	0.50	0.110	Salt
18	14	4.13	140	38.7	30.5	3.40	0.68	0.090	Salt-sug
19	17	5.02	120	38.0	27.0	5.40	0.48	0.130	Salt
20	17	5.02	110	41.0	30.6	4.40	0.60	0.120	Salt-sug
21	20	5.90	80	38.0	26.0	5.50	0.43	0.120	Salt
22	20	5.90	100	40.5	29.7	4.85	0.55	0.110	Salt-sug
23	5 ($H = 0.1$)	0.733	1800	20.8	21.0	0.50	0.40	0.04	Salt-sug
24	5 ($H = 0.1$)	0.733	1800	24.0	23.0	0.40	0.20	0.04	Salt
25	5 ($H = 0.1$)	2.93	1200	24.0	23.0	0.60	0.50	0.09	Salt-sug

TABLE 1. Measured quantities in the experiments: source volume flux Q, buoyancy flux F, intrusion formation period P, shear layer depths D_i for the first two layers above the bottom outflows, corresponding shear layer velocities U_i, and filling-box vertical velocity V, as defined in the text. Also listed is whether the run used two salt plumes (Salt) or one salt and and sugar plume (Salt-sug). The values given for layer depths and velocities are averages over at least four measurements. The errors tend to be larger in experiments with small buoyancy fluxes as a result of slower time variations. All runs had a plume height of fall $H = 0.2$ m, except three runs with $H = 0.1$ m as shown in column 2.

largely two-dimensional. The novel aspect to be reported here is that interleaving intrusions led to extensive mixing between the two halves of the channel.

Single-component experiments, using two identical salt sources but with trace concentrations of dye in one source, provided the key results. However, two-component experiments were also carried out in order to examine the relative roles and interaction of double-diffusive convection and internal wave motions. We aimed to achieve conditions ranging from those dominated by waves to those dominated by convection. Heat–salt experiments proved unsuitable for quantitative measurements for a number of reasons. Thus we used the salt–sugar analogue to heat and salt, with very small source volume fluxes and large source concentrations. The two-solute system also involved thinner salt-finger regions and tends to scale better to other flow features in the laboratory than does the heat–salt system.

Thirty quantitative experiments were carried out (table 1). The volume flow rate Q through the nozzles was generally fixed (at 5 ml min $= 8.3 \times 10^{-8}$ m^3 s^{-1}), but the density of the sources was varied in order to vary the buoyancy flux. To achieve the largest buoyancy fluxes used the flow rate was increased (to 20 ml min^{-1}). At

these volume fluxes the water depth increased slowly with time (refill time of 45 to 180 hours). However, this was considered to have negligible effect given the much smaller time (up to 30 min) taken to cycle the box volume through the plumes and generate a density gradient of constant shape. Other quantities of relevance were the individual contributions to $\Delta\rho$ from sugar ($\beta\Delta S$) and salt ($\alpha\Delta T$), where $\beta = (1/\rho)\partial\rho/\partial S$ and $\alpha = (1/\rho)\partial\rho/\partial T$ are the solutal expansion coefficients for sugar (S) and salt (T), the molecular diffusivities κ_S and κ_T of sugar and salt, respectively, the kinematic viscosity ν, the dimensions of the channel (length L and width B, where the latter is relevant in setting the volume to be ventilated by the plumes), and the height of fall H from the plume source to the bottom. The important governing parameters in the single-component experiments are the Prandtl number $Pr = \nu/\kappa_T$, aspect ratio H/L and a Reynolds number $Re = UD_1/\nu$ (which we define in terms of the internal quantities U_1, the horizontal speed, and D_1, the thickness, of the second intrusive layer from the bottom, which we also refer to as the first shear layer above the bottom outflows; see figure 1 for definition sketch). For two-component cases there are, in addition, the density ratio $R_\rho = \alpha\Delta T/\beta\Delta S$ and diffusivity ratio $\tau = \kappa_S/\kappa_T = 1/3$. We carried out experiments with a range of buoyancy fluxes, a range of concentration contrasts ΔS, and two values of the height H. We did not vary the tank length L. The effect of length L on the internal waves was tested in WGH01 for the case of a single plume. The experiments were confined to cases in which the tank was initially filled with fresh water and the two plumes had equal buoyancy and volume fluxes within the measurement or instrument uncertainty. In two-component runs one plume source contained only salt and the other only sugar, hence $\alpha\Delta T = \beta\Delta S$. In this way the potential role of double-diffusive convection was maximized.

The flow was visualized using a shadowgraph screen and recorded on video. The flow was largely two-dimensional in most of the channel. However, measurements were complicated by some variation across the width of the channel near the front. By adding trace amounts of food colouring to one of the sources the interface between waters from the two plumes, at least in the single-component case, could be defined for a time of the order of the ventilation time, and much longer near the base of the tank. In double-diffusive cases the convective mixing reduced the usefulness of the dye in revealing intrusions beyond their early stages of growth. In both single- and two-component cases, the dye eventually recycled through both plumes and became increasingly evenly distributed throughout the box. Horizontal velocities and vertical length scales of shearing were measured by dropping dye crystals, which produced vertical dye lines, and monitoring the subsequent distortion of the dye lines. Vertical advection of dyed layers was measured to find the vertical velocity. The period of oscillations of the front was measured in real time or from the video record. A suction conductivity probe (Bidokhti 2000) was used to measure profiles of conductivity with depth in some runs, and to monitor the temporal changes in conductivity at fixed points in the flow.

A few additional qualitative experiments were carried out in tanks of different size or shape (including a cylindrical tank) in order to determine whether the formation of shear layers by internal waves could be suppressed relative to double-diffusive convection. However, we were unable to find a method that removed the strong layering due to internal wave modes. A reduction of the plume buoyancy flux or the height of fall of the plumes reduced the plume volume flux at the base of the tank and hence the horizontal velocities, as predicted by WGH01. However, single-component runs with a plume height of fall of as little as 0.1 m and the smallest buoyancy flux that was practical to measure (i.e. conditions giving the weakest internal wave

forcing) still showed the interleaving structure. In a few runs a small horizontal disk was mounted close to the source, increasing the effective size of the source and causing turbulent mixing into the plumes closer to the source. This had no measurable effect on the circulation and frontal interleaving. A few runs with heat and salt (using one cold plume and one salty plume) showed vigorous salt-finger convection in which the layers were thicker than those in the salt–sugar experiments, indicating a possible stronger role for double-diffusive convection in setting the layer thickness than will be reported here for the salt–sugar experiments. Source density anomalies in heat–salt runs were also much smaller, and hence internal wave motions were relatively weak. Heat gain through the sidewalls was not a substantial issue given the very large convective fluxes between layers. However, the rapid vertical fluxes and long salt fingers in these runs meant that the layer thickness, velocities and water properties could not be measured satisfactorily.

3. Qualitative observations

Figure 2 shows photographs of the flow in two experiments with the same buoyancy flux, for a single solute (*a*) and with two solutes (*b*). The dye lines revealed nearly symmetric horizontal velocities on each side of the front. In the two-component case the dye that was added to the salt source approximately marks the distribution of salt concentration throughout the tank. In the single-component case the dye is the only thing making visible the front, the interleaving intrusions and the eventual horizontal layering. In the two-component case the differing effects of salt and sugar on the refractive index (at the same density) provided additional refraction effects in the shadowgraph images.

The position of the confluence between the two plume outflows at the base lay close to the mid-point of the tank length and varied with time by only a few centimetres. At first sight the filling-box circulation and horizontal shear layers on the two sides of the front formed a symmetric flow, similar to that obtained if a solid boundary was inserted at the centre of the tank. As implied in figure 1, such a flow is expect to involve a wave mode (see WGH01) that is stationary relative to the box and whose amplitude decays with height. This dominant wave mode will have nodes of vanishing horizontal velocity at the centre and each end of the box, and these will be superimposed on the mean circulation involving a depth-dependent horizontal entrainment velocity into each plume. The entrainment flow must vanish at the mid-point of the channel, and therefore at the centre of the front. The number of shear layers was between four and six, consistent with the observations and theory of WGH01. Occasionally there was one layer more on one side of the front than the other. However, it was difficult to define how often this was the case or how it came about.

On the other hand, the flow close to the front was neither steady nor exactly symmetrical about the mid-point of the tank. This was particularly obvious at depths slightly above the bottom outflows (1/3 to 1/2 of the height to the plume sources). At this height the velocity oscillated in direction, with periods ranging from 100 s to 1800 s (table 1). The oscillations carried the tracer or compositional interface alternately back and forth. A new intrusion to the left or right was formed on each half of this oscillation. At the same time the water column, with the intrusions, was advected upward by the mean circulation. Thus the sequence of oscillations gave rise to a series of intrusions interleaving across the front. The overall appearance was that of a spatially developing disturbance whose amplitude grew with height (i.e. in

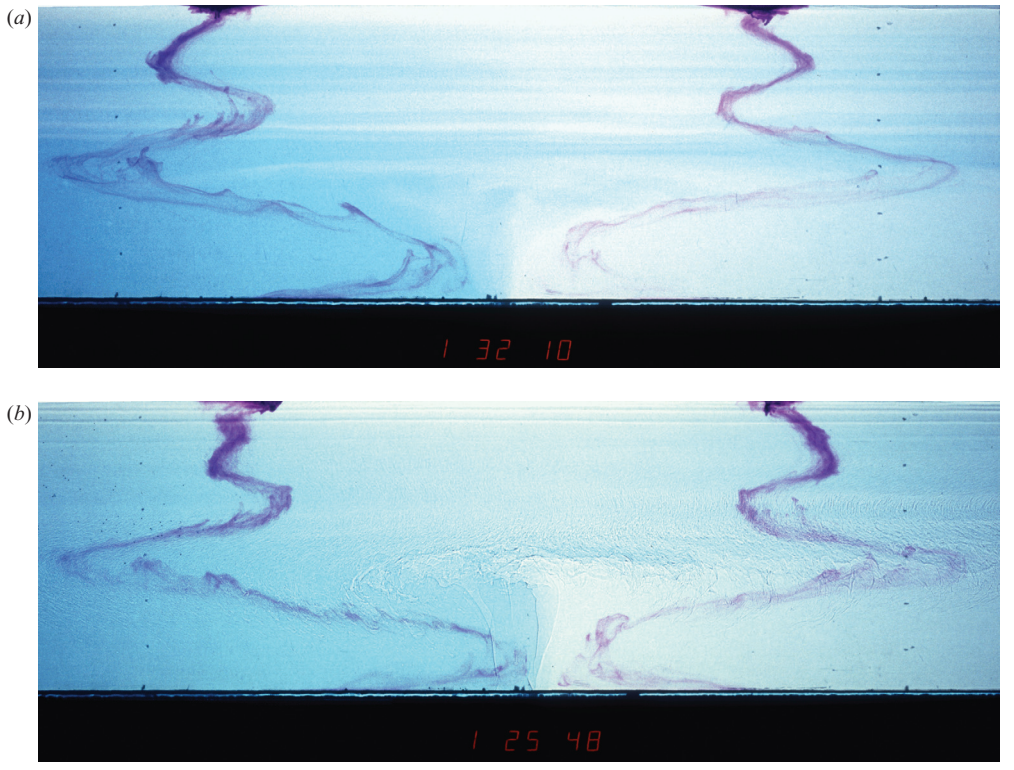

FIGURE 2. Photographs of (*a*) a single-component case (two identical salt plumes) and (*b*) the corresponding two-component case (the right-hand plume source was a sugar solution, the left-hand source was a salt solution). Double-diffusive convection, salt fingering and 'diffusive' interfaces were vigorous in (*b*). The horizontal displacements of two $KMnO_4$ dye lines indicate the profile of horizontal velocity in the shear layers, and are nearly symmetric about the middle of the channel. The blue dye is a passive tracer that was added to the left-hand plume source long after the filling-box density gradient had been established, and the photographs were taken at a time after the dye had entered the interior and been carried to the top on the left-hand side by the upward flow. At this time some of the dye (and salt in (*b*)) had also been entrained into the opposite plume via the horizontal intrusions and recycled into the right-hand cell. Photographs taken at (*a*) 1 h 32 min – a rightward moving intrusion has formed and the next leftward intrusion is about to commence, (*b*) 1 h 26 min after the start – a leftward intrusion is growing. The buoyancy flux in each plume was $F = 1.92 \times 10^{-7}\ \mathrm{m^4\,s^{-3}}$ and plume height was $H = 0.2$ m.

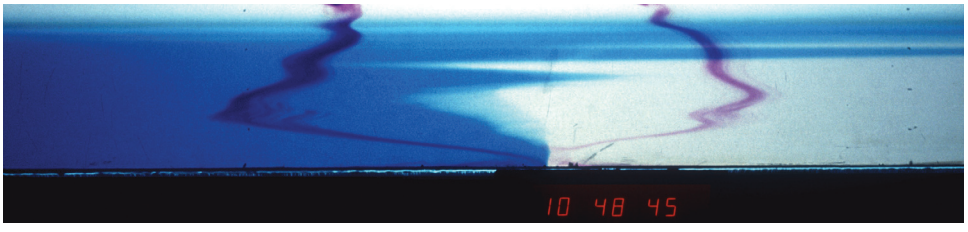

FIGURE 3. A photograph of a single-component experiment the same as that in figure 2(*a*) but with a smaller plume height ($H = 0.1$ m). The addition of blue dye (a passive tracer) to the left-hand source was again commenced long after the filling-box density gradient had been established. The photograph was taken 10 h 49 min after the sources were turned on. The time elapsed between commencement of dye input and this photograph was shorter than in figure 2(*a*) so that the dye concentration in the right-hand side of the channel was smaller.

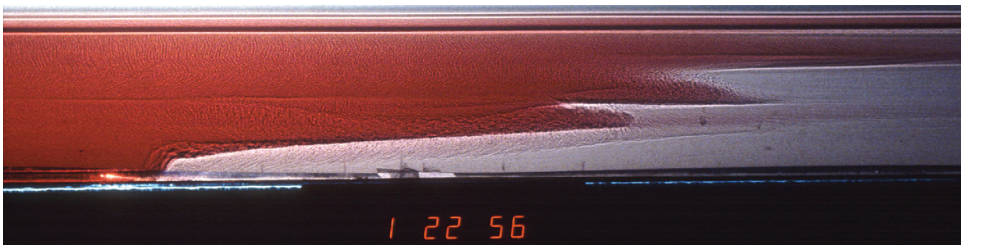

FIGURE 4. A photograph of a sloping T–S front in an experiment with salt (left) and sugar (right) plumes having a buoyancy flux of approximately $F = 2.93 \times 10^{-7}\ \mathrm{m^4\ s^{-3}}$ and an effective height of $H = 0.1$ m. A disk of 18 mm diameter was attached to the plume nozzles to increase the source size and amount of entrainment into the plume. New interleaving intrusions are continually formed and advected upward. The 'front', or concentration interface, at the base was stationary in the position seen here apart from small oscillations.

the direction of the mean flow). A direct relationship between the velocity field and the compositional field was clear near the base and immediately above the bottom outflows, where the intrusions formed. Furthermore, as each new intrusion grew (say, a salty intrusion moving to the right), there was a simultaneous decrease (and often a reversal) in the rate of extension of the preceding intrusion of the same sign (the previous salt intrusion). Thus the extension rate of intrusions was not monotonic. This was consistent with the advection of intrusions upward to where the quasi-stationary shearing layers had a horizontal velocity in the opposite direction. At larger heights each compositional intrusion eventually became a layer extending from end to end of the box and they grew thinner as they were advected upward. The entrainment velocities into the plumes are expected to have become significant in helping to stretch the intrusions once they extended far from the centre of the channel. At these heights we were unable to track the complicated interactions of the intrusions with the decaying shear layers, but it was clear that the upward-moving compositional layers became much thinner than, and passed through, the stationary shear layers. We also note that dye injected in the plumes showed that there was no detrainment from the plumes into any of the shear layers above the bottom outflows. Rather, vertical dye lines near the plumes showed that entrainment occurred at all depths, consistent with previous studies of vertically falling plumes in filling-box gradients and in line with the prediction that the dominant wave mode has zero horizontal velocity at the endwalls.

In the single-component experiments there was no mixing between or within the horizontal intrusions. For a period after adding dye to one plume, the intrusions in one direction carried dye (diluted by entrainment into the dyed plume) whereas intrusions in the opposite direction carried no dye. The vertical density gradient was indistinguishable from the smooth filling-box gradient. Figure 3 shows a single-component experiment with the smaller plume height, and the behaviour was qualitatively similar to that in figure 2. In the upper region of the stratification, each intrusion extended all the way to the opposite plume. Hence the dye began to be entrained into the opposite plume. The dye was thereafter recycled through both plumes. At these heights the intrusions no longer had a leading edge and we therefore refer to them as layers (a term which here carries no implication of internal mixing or modification of the density gradient). Importantly, the decreasing difference in dye concentration across the front represents a net horizontal transport due to the interleaving.

In the two-component experiments illustrated by figure 2(*b*) the sequential formation of intrusions in alternating directions appeared to be similar to that in the single-component case. However, the compositional difference caused intrusions interleaving towards the right to be richer in salt and those moving to the left richer in sugar. The intrusions were again advected upwards through the wave fronts, and again became thinner owing to entrainment into the plumes. Double-diffusive convection was vigorous, with regions of salt fingers alternating with sharp diffusive density interfaces in a manner similar to the interleaving layers of the Ruddick & Turner (1979) dam-break experiments. The most prominent features on the shadowgraph screen were therefore a salt-finger region below the most recently formed leftward moving (sugar rich) intrusion and a diffusive interface below the most recently formed rightward moving (salty) intrusion. A consequence of the vanishing horizontal density difference was that the local double-diffusive stability ratio $R_{\rho local} = \beta\delta S/\alpha\delta T$ across the quasi-horizontal interfaces (where δS and δT are the local vertical concentration differences) was very close to one. Hence the salt finger convection was vigorous and caused the dye to quickly mix between adjacent layers. The net buoyancy flux associated with the convection caused the layers to slope noticeably (downward in the direction of higher sugar concentration) relative to horizontal density surfaces. The vertical profiles of horizontal velocity were similar to those in the single-component experiments.

The Reynolds number ($Re = UD_1/\nu$) of the flow in the first shear layer above the bottom outflows (see figure 1) was of order 100. Thus viscous stresses are expected to influence the horizontal velocities, and particularly the decay of shear layer strength with height (as predicted by WHG01). In single-component runs the flow outside the plume and the bottom outflow was generally entirely laminar, except that in runs having the largest Re a small amount of mixing could be seen near the nose of the first intrusion above the outflows.

In some runs using the smallest buoyancy flux or the smaller plume height, the flow was asymmetric with a sloping mean orientation of the front, as illustrated in figure 4. The slope can be attributed to slightly unequal plume buoyancy fluxes (largest on the right), the larger flux giving a stronger outflow at the bottom and more rapid entrainment at other levels. As with the vertical fronts, sloping fronts periodically developed a new intrusion near the level of the first shear layer above the outflows and the intrusions extended as they moved upward.

4. Measurements

Flow measurements were taken from the video record for times after the plumes created a steady density profile throughout the volume below the level of the sources (30 min) and before the water depth in the box increased by 20 mm (18 hours). We focused on a small number of specific aspects of the flow (listed in table 1) that were relatively clearly defined (see figure 1). They included: (i) the horizontal speed U_1 of flow towards the plumes in the first shear layer above the plume outflows (the maximum in many sequential velocity profiles centred at 200 mm each side of the mid-point of the channel were averaged); (ii) the horizontal speed U_2 of flow away from the plumes in the second shear layer above the outflows (again an average from many sequential profiles); (iii) the thicknesses D_1 and D_2 of the first and second velocity layers, respectively (averaged over measurements taken at the same times as the velocities); (iv) the period P of intrusion formation, defined as the time between two consecutive intrusions in the same direction; and (v) the vertical advection velocity V of the compositional intrusions, measured at mid-depth and taken from the migration

of horizontal interfaces. The horizontal entrainment velocity into the plumes was not measured, as this would require fitting a theoretical profile through the alternating shear layer velocity structure at a chosen horizontal location. We instead rely on the theoretical solution for a filling-box flow and consistency of the volume flux with that implied by the measured vertical velocity at mid-depth.

These measurements can be compared with the theory of WGH01 for inviscid travelling wave modes that are held stationary in the box by the upward filling-box advection. The theoretical plume outflow velocity in dimensional form is

$$U_0 = u_0(2E)^{4/3}\pi^{2/3}H^{5/3}F^{1/3}A^{-1}, \tag{4.1}$$

where

$$u_0 = 0.254 m_0 H L/(L-x) \tag{4.2}$$

is a dimensionless velocity scale, H is the effective depth of the plume, L is the length of the tank (and $L/2$ is the effective length of cavity filled and excited by each plume), x is the horizontal distance from the plume, A is the surface area of the tank (taken as half of the full tank area for each plume), E is the plume entrainment coefficient (taken to be 0.13 since the theory here is based on the top-hat profile across the plume, and this number corresponds to 0.091 for a Gaussian profile; Turner 1986), and $m_0 H$ is the non-dimensional vertical wavenumber at the bottom of the tank (noting that the analysis assumes the buoyancy frequency varies slowly with height). The wavenumber at the bottom is found to be

$$m_0 H = 2.02(2E)^{-1}(W/H)^{1/2}, \tag{4.3}$$

where W is the width of the tank (which enters through the tank volume to be cycled through the plume). For our experiments $L/(L-x) = 2$ and we evaluate $u_0 = 3.4$ and $m_0 H = 6.4$. Equation (4.1) over-estimated (by about 20 %) the outflow velocity in the previous experiments with a single plume. It again over-estimates these in the present experiments by an amount that increases with decreasing buoyancy flux. The difference is likely to be a result of viscous stresses (noting that WGH01 also found a solution for the viscous flow with a uniform buoyancy frequency). The overlying shear layer speeds U_1 were approximately 15 % smaller than the outflow speeds. The values of U_1 in cases with double-diffusive convection were systematically about 25 % smaller than those in the single-component cases.

All velocities were measured at 200 mm from the mid-point of the channel, where there was no significant entrainment velocity toward each plume. Even at positions 1/4 and 3/4 of the distance along the channel from one end, the filling-box solution together with the internal wave model of WGH01 predicts a ratio of the bottom outflow speed U_0 and the entrainment speed u_e as $U_0/u_e = 6$ (using equations (5), (6) and (45) of WGH01). Hence entrainment plays only a weak role in the growth of the observed intrusions. Both shear layer and entrainment velocities decay with height, but the shear layers decay fastest at these Reynolds numbers, and the intrusions also extend closer to the plumes as they move upward. Hence entrainment plays a greater role in the continued stretching of intrusions in the upper parts of the stratification.

In the second shear layer above the outflow the speeds U_2 were an order of magnitude smaller than U_1. The effect of double-diffusive convection was again to reduce the velocities by around 20 %. According to the theoretical solutions of WGH01, the difference between the two shear layers can be attributed partly to the density gradient (which increases with height) and partly to the effects of viscosity. In particular, the predicted exponential scale height for decay of the

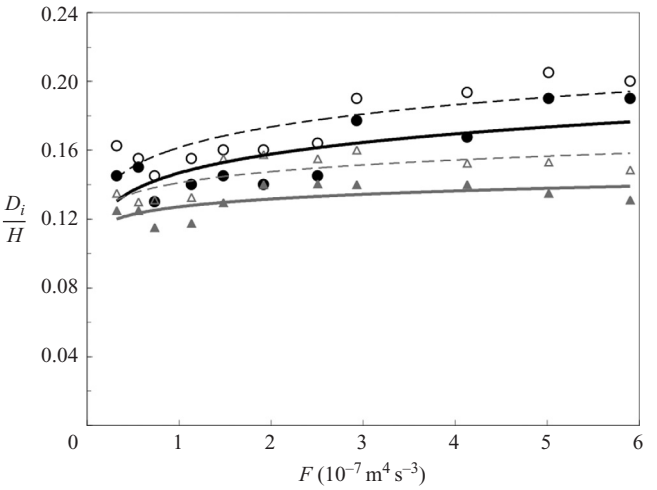

FIGURE 5. The thickness of shear layers inferred from the vertical profiles of horizontal velocity, as a function of plume buoyancy flux F for cases with $H = 0.2$ m. Filled circles, solid black line: shear layer 1, single component; open circles, broken black line: shear layer 1, two-component; filled triangles, solid grey line: shear layer 2, single component; open triangles, broken grey line: shear layer 2, two-component. The lines are best-fit power-law curves and serve as only a guide to read the data.

velocity amplitude of shearing modes in a viscous fluid having uniform buoyancy frequency is $\beta = 2\pi H Re_H (H/L)/(m_0 H)^4$, which is dependent on the Reynolds number $Re_H = N_b H^2/\nu$. As N_b and Re_H are smaller for smaller plume fluxes, so the decay height decreases with F. For the present experiments the dimensionless decay height is in the range $0.3 < \beta/H < 0.82$, which indicates the observed rapid decrease of velocity with height.

The measured vertical advection velocity V of the compositional layers near mid-depth (table 1) was consistent with the predicted filling-box solution (Baines & Turner 1969),

$$V = (2E)^{4/3}\pi^{2/3}H^{5/3}F^{1/3}A^{-1}[0.46(z/H)^{5/3} - 0.059(z/H)^{8/3} - 0.01(z/H)^{11/3} + \cdots], \quad (4.4)$$

over the range of buoyancy fluxes used, where the area A is again taken to be half of the area of the channel to allow for the two plumes.

The thickness of the plume outflows in all runs was 1/4 to 1/3 of the plume height of fall, as in WGH01 and consistent with the hypothesis that the thickness is governed by the internal wave dynamics. The interior circulation V and the buoyancy frequency N of the filling-box flow (see (4.5) below) both vary as $F^{1/3}$, and hence the inviscid vertical wavenumber (and outflow thickness) is independent of buoyancy flux. However, our interest here is in the thickness of the shear layers and intrusions above the outflows. The thickness of the shear layers, derived from the velocity profiles and normalized by H, are shown for the first two layers in figure 5. For single-component runs (filled symbols) the thickness of the first shear layer (circles) increased weakly with buoyancy flux, whereas the second shear layer was slightly thinner and varied less with F. This variation is consistent with (4.3) and a smaller entrainment constant for the small buoyancy fluxes, at which the plumes were not fully turbulent near the source. The newest intrusion, on the other hand, was always coincident with the first shear layer and its initial thickness was comparable to the shear layer thickness.

Both the first and second shear layers were approximately 15 % thicker when double-diffusive convection was present (open symbols in figure 5). This appeared to be a result of convection (which was not confined to the intrusions as an unavoidable result of recycling of interior water through the plumes), although double-diffusive instability within the plume might also have caused a greater entrainment rate and larger volume outflow.

We examined two Froude numbers, U_i/N_bD_i and U_i/N_bH based on the measured shear layer horizontal velocity and thickness, for each of the first and second shear layers ($i = 1, 2$), where N_b is the buoyancy frequency at the bottom ($z/H = 1$) predicted by the previous filling-box solution (see WGH01)

$$N = F^{1/3}(2E)^{-2/3}\pi^{-1/3}H^{-4/3}\left[2.18(z/H)^{-5/3} + 0.279(z/H)^{-2/3} + 0.0831(z/H)^{1/3} + \cdots\right]^{1/2}. \quad (4.5)$$

Figure 6(a) shows the Froude number values U_i/N_bD_i for both the first shear layer (circles) and the second shear layer (triangles), while figure 6(b) shows U_1/N_bH for the first shear layer only. Also shown as a horizontal line in figure 6(b) is the Froude number for the plume outflow predicted by the inviscid theory for shearing modes (labelled 1 and 2). The measurements show that, for a single-component flow (solid symbols) and the larger plume buoyancy fluxes used ($Re_H > 5000$), the speed in the first shear layer was equal to that predicted for the bottom outflow layer, with $U_1/(N_bH) = 0.14$. The layer Richardson number, $Ri = (N_bD_i/U_i)^2$, in the first shear layer is smaller than the expected critical value of 0.25 for shear instability, and consistent with the observation of some instabilities there. At smaller buoyancy fluxes the Froude number was smaller and, as above, we attribute this to viscous effects.

The intrusion formation period P (see table 1) is plotted in both dimensional and normalized forms in figure 7. In figure 7(b) P is normalized by the time scale $T_w = N_bD_1L/2$ for internal waves of vertical wavelength $2D_1$ to travel the length L of the channel assuming a buoyancy frequency predicted by (4.5) evaluated at the bottom. The intrusion period decreases with increasing buoyancy flux (the power law of best fit is $P \sim 225F^{-0.57}$), whereas the normalized periods are close to constant at order one times the wave travel time. The periods are much smaller than the time scale for vertical advection in the filling-box circulation, with an average of $P = 0.07H/V_b$, where $V_b = V(z/H = 1)$ is obtained from (4.4). The addition of double-diffusive convection (open circles) in most cases increased the period by an average 20–30 %, a change we attribute to the increased shear layer depth.

Time records of conductivity were taken from probes placed at the middle of the first shear layer and 1/3 of the distance from either end of the channel, so as to detect the sequential formation of salt- or sugar-rich intrusions towards the opposite plume. Figure 8 shows time records of salty intrusions toward the sugar plume, for runs with two different buoyancy fluxes. The oscillatory formation of intrusions at the mid-point of the channel created a series of conductivity peaks (salt intrusions) and troughs (sugar intrusions). These were superposed on a slow secular trend that represents the continued addition of salt to the tank. The time between two consecutive peaks (approximately 200 s and 1700 s for the experiments in figure 8) was consistent with the intrusion period P measured from the videos (200 s and 1800 s; table 1) and comparable to the time for the longest internal waves to travel the length of the tank. Higher frequencies in the time records were a result of turbulent mixing at the upper edge of the plume outflows.

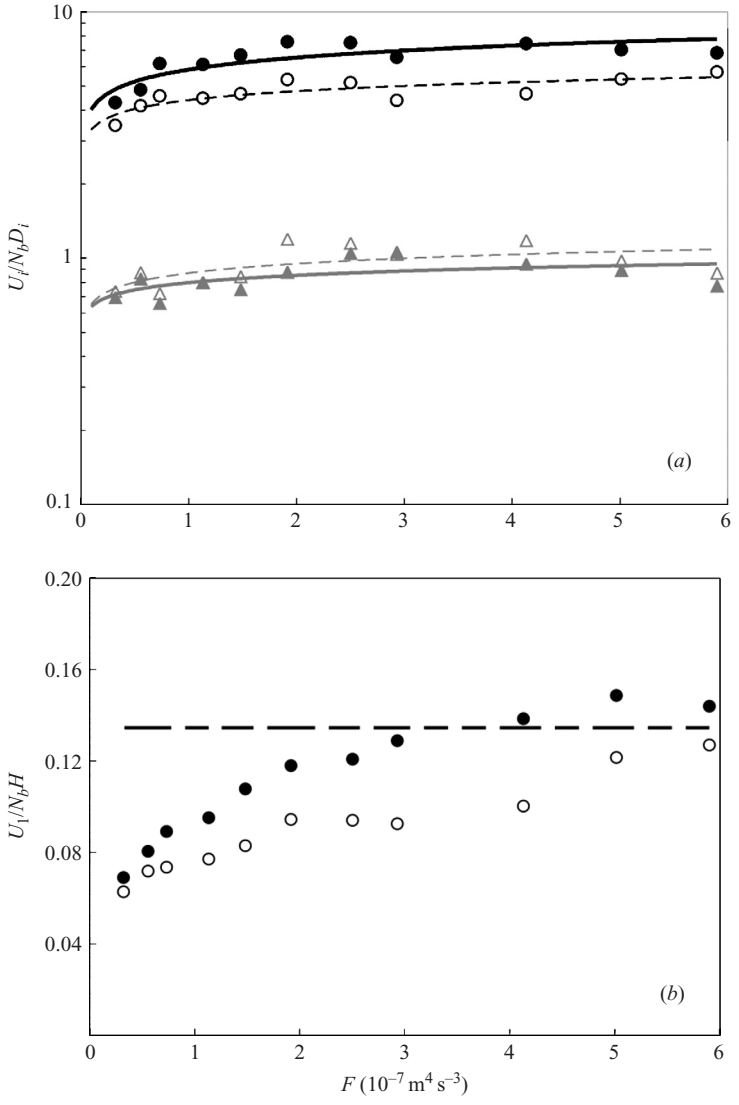

FIGURE 6. Froude numbers for the shear layers defined using (*a*) the layer thickness D_i or (*b*) the depth H of the stratified water (for runs with $H = 0.2$ m). Symbols are as in figure 5: circles, first shear layer; triangles, second shear layer: solid symbols, single component; open symbols, double-diffusive cases. Curves show the power laws of best fit as a guide. In (*b*) only the results for the first layer are plotted. For comparison the Froude number predicted for the bottom outflow by WGH01 is plotted (horizontal broken line). Note that these data are based on the total velocities, which are the sum of the entrainment velocity into the plumes and the shear layer velocity profile at the height of the first shear layer at the position of measurement.

Vertical profiles of conductivity in single-component runs revealed the large-time asymptotic profiles characteristic of the filling-box process. Perturbations to this underlying density and conductivity profile due to shear layers and intrusions were too small to identify, as these involved no mixing or formation of density steps. For two-component cases, however, conductivity profiles revealed the lateral intrusions of differing salinity. Figures 9(*a*) and 9(*b*) show profiles from the sugar side and salt

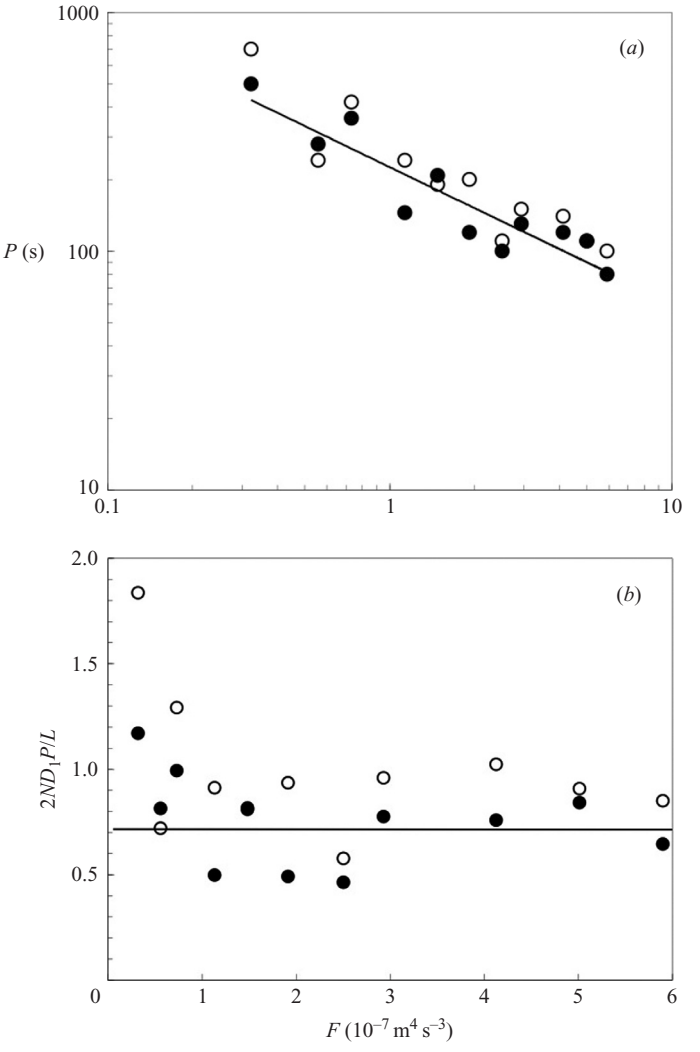

FIGURE 7. (*a*) The period P of formation of interleaving intrusions (taken as the time between two consecutive intrusions in the same direction) for runs with $H = 0.2$ m, along with the power law of best fit to the single-component cases ($P \sim 225F^{-0.57}$); (*b*) the period P normalized by the approximate travel time over a distance L for an internal wave of wavelength $2D_1$. Symbols indicate single-component (filled circles) and two-component (open circles) cases. The horizontal line in (*b*) at a value of 0.73 shows the average of all runs with buoyancy flux $F > 10^{-7}$ m^4 s^{-3}.

side, respectively, for one experiment, where the profiles were taken long after the filling-box density profile had been established. As the effect of sugar on conductivity is negligible for the range of concentrations in these experiments, the profiles were substantially different on the two sides of the front. Salt-rich intrusions in a largely sugar concentration gradient (figure 9*a*) presented a large conductivity contrast, despite the double-diffusive fluxes which significantly reduced the vertical contrasts. In comparison the sugar-rich intrusions on the other side of the front (figure 9*b*) contained a concentration of salt that was not substantially different from that into which they intruded. The five main conductivity maxima and minima matched the

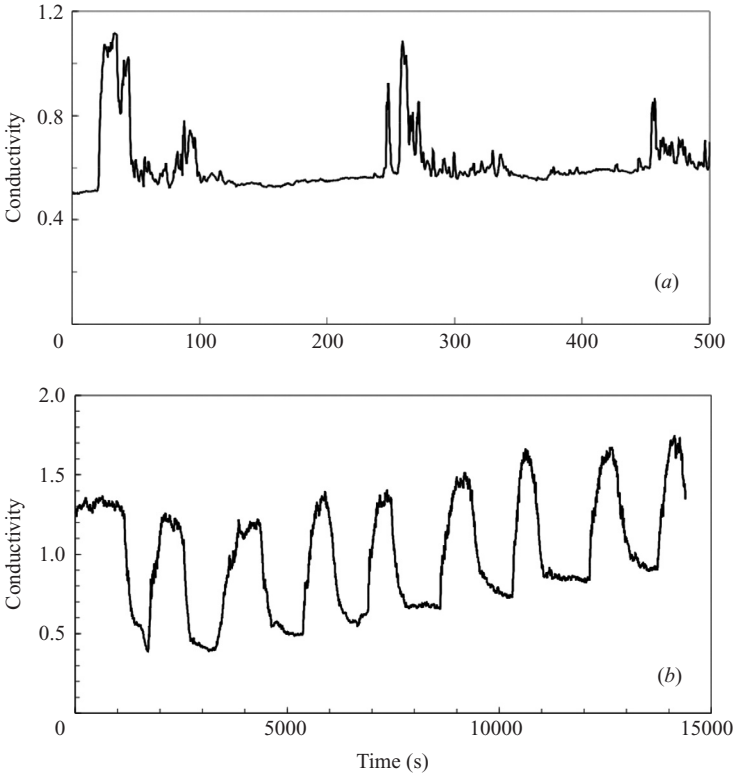

FIGURE 8. Continuous records of conductivity from (*a*) a probe fixed at 0.3 m from the mid-point of the tank and $z = 85$ mm from the bottom on the sugar plume side of the front ($H = 0.2$ m and $F = 1.9 \times 10^{-7}$ m^4 s^{-3}), and (*b*) a probe fixed at 0.3 m from the front on the sugar plume side and $z = 50$ mm from the bottom ($H = 0.1$ m and $F = 0.73 \times 10^{-7}$ m^4 s^{-3}). In each case the position of the probe was close to the height at which the intrusions formed. There is a secular trend in the baseline as a result of an increasing total amount of salt in the tank.

observed dye tracer locations at the same times. The shearing layers identified from the velocity field approximately matched the first three maxima and minima above the outflow. However, the conductivity profiles reveal more structure than do the velocity profiles.

5. Discussion

The interleaving phenomenon reported here cannot be driven by the mechanisms of layer formation that are active in sidewall heating of a salinity gradient (Chen & Chen 1997), the instability of a turbulent front (Browand *et al.* 1987), or double-diffusive instability of a front (Ruddick *et al.* 1999). In those cases the intrusions are driven by local buoyancy forcing and the vertical scale is governed by either the imposed density differences (in sidewall heating and double-diffusive cases) or the Ozmidov scale at which buoyancy suppresses turbulence (in the case of a spreading turbulent front). These cases also involve no role for internal waves other than the zero-frequency mode (the upstream wake) generated by the intrusions themselves. In the present case the turbulence in the plumes had frequencies larger than the surrounding buoyancy frequency and, like the grid turbulence in experiments such as those of Browand

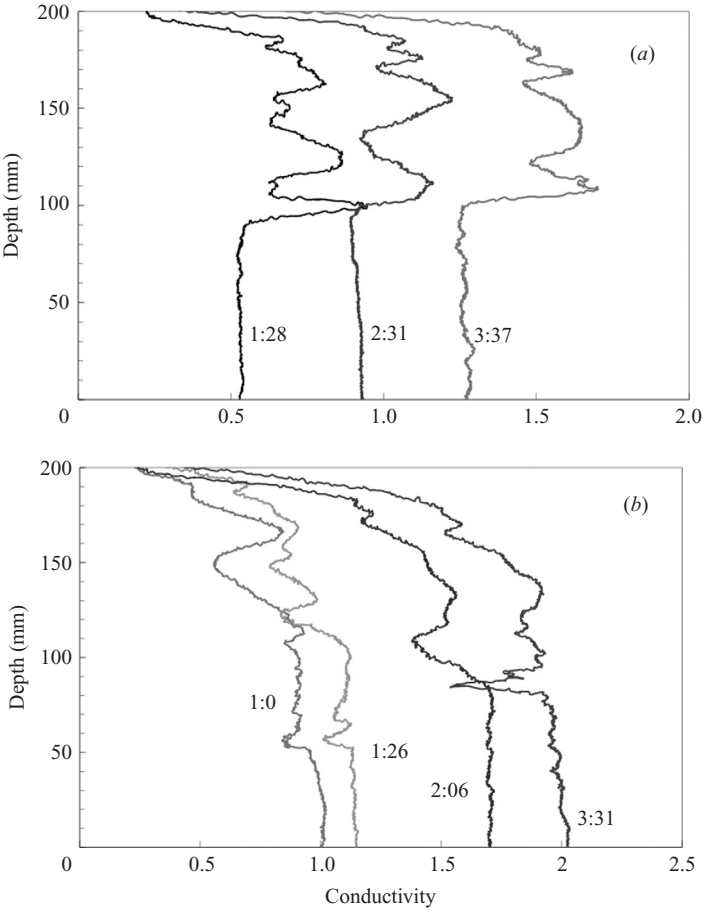

FIGURE 9. Vertical profiles of conductivity from an experiment with sugar and salt plumes having $F = 2.93 \times 10^{-7}\,\mathrm{m^4\,s^{-3}}$, and $H = 0.2\,\mathrm{m}$. Profiles were taken (*a*) on the sugar plume side of the front and (*b*) on the salt plume side, both at 0.3 m from the mid-point of the channel. Times after the start of the experiment are shown in hours:minutes. Conductivity is in arbitrary units (which are actually the voltage output from the conductivity apparatus that is linear with conductivity). Although conductivity profiles reveal salty intrusions most clearly, both sides of the front exhibit more complicated compositional fine structure than that seen in profiles of horizontal velocity. Smoothing the profiles in (*b*) also indicates the overall shape of the salinity and density profiles.

et al. (1987), could not generate significant wave motion. Furthermore, owing to the buoyancy fluxes in the plumes, the plume turbulence could not collapse as intrusions into the surrounding density gradient. Thus the only effect of the turbulence was its contribution, through entrainment, to the mean filling-box circulation. In contrast, the compositional intrusions originated at the mid-point of the channel. In the absence of a horizontal density or property difference across the front, the only available driving for motions at the front was the buoyancy-forced motion of the plume outflows at the base. Each of the outflows excited the travelling wave modes described by WGH01, and potentially also modes that are not symmetric about the mid-point, and these wave motions in turn generated the sequence of intrusions. Once the intrusions extended far from the mid-point, and were carried to the upper parts of the water

column, the entrainment flow into the plumes began to play an increasing role in enhancing the continued stretching of the intrusions. In this way the entrainment acted as an extensional flow surrounding the front. It caused the intrusions to become thinner (along with increasing the density gradient) as they approached the height of the plume sources.

A simple application of the internal wave solutions described by WGH01 to the present experiments with two plumes would assume symmetry about the mid-point of the box, with a node in the horizontal velocity at the centre and each end of the box. However, in the realized flow the symmetry is broken and there is instead an oscillatory horizontal velocity at the mid-point. Small perturbations from perfect symmetry in either the density or the velocity field are expected to lead to lateral displacements of the vertical interface between the two water masses, but the cause of the oscillation remains unclear. An oscillation was also observed in the single-plume experiments of WGH01, seen as fluctuations in conductivity at any point in the interior of the flow and as a fluctuation in the number of shear layers (usually cycling between four and five layers). The period in that case was close to 2000 s in a box of comparable dimensions, but it was not clear how the period scaled. If we apply the same normalization of the period as used in the present experiments (figure 7*b*), allowing for all of the tank volume to be recycled through the single plume, we obtain values consistent with those found here. Hence the mechanism responsible for intrusion formation, though as yet unidentified, may have been present in the simpler case of a single plume falling into a long box. We speculate that this may involve the presence of a wave mode having double the horizontal wavelength of the dominant mode, which in the present case of two plumes suggests a mode having a maximum velocity at the mid-point of the channel. This mode would carry the front back and forth. The observed oscillations require that such a mode have a vertical wavelength comparable to the dominant mode, presumably because it must derive energy from the bottom outflows. The period of such a mode would be consistent with the constant value of order one found from the normalization of measured periods in figure 7(*b*). As a consequence of not being stationary relative to the box, it would not be forced as strongly as the dominant mode.

The single-component experiments reveal that interleaving intrusions formed even when the shear layer flow was laminar. Hence no vertical mixing or local overturning was required. When double-diffusive convection was present it caused vertical mixing within each intrusion, and involved the formation of salt fingering and diffusive density interfaces with associated vertical fuxes between intrusions. Beyond this, the convection led to only slightly thicker interleaving layers and a minor reduction of the horizontal velocities. These effects of convection might be attributable to increased friction between layers (Maxworthy 1983; Ruddick 1985; Ruddick, Griffiths & Symonds 1989), the altered density structure within the intrusions, or vertical buoyancy fluxes. The key point, however, is that layer thickness and intrusion extension rates remained strongly governed by the internal wave dynamics.

By way of contrast, the normalized speed of interleaving layers in 'dam-break' double-diffusive front experiments (Ruddick & Turner 1979; Ruddick *et al.* 1999) was very much smaller than the velocities measured in the present experiments: the Froude number was found to be $U/(ND) \sim 0.005$ (where U and D are the velocity and depth of the interleaving intrusions), whereas the present internal wave forcing gives $U_1/(N_b D_1) \sim 7$ (figure 6*a*). The flow structure in the present experiments appeared most similar to that seen in the 'dam-break' experiments when we used the smallest plume buoyancy fluxes. Under these conditions the relative effects of

double-diffusive convection appeared stronger, in that the interleaving layers sloped more strongly (downwards towards the sugar-rich side) and the leading edge of each intrusion showed the curved and pointed feather shape characteristic of double-diffusive intrusions. At larger plume fluxes the layer slope was not measurable and the intrusions had more rounded leading edges. We note that a clear definition and parameterization of the relative roles or strengths of double-diffusive convection and internal wave displacements has been elusive, a point that is important when attempting to extrapolate results from the laboratory to the oceans.

6. Conclusions

Vertical density stratification and a density-compensated horizontal property (or tracer) gradient were produced and continuously maintained, in a uniform vertical flow, while being subjected to low-frequency travelling wave modes. Lateral wave displacements within the horizontal gradient generated an alternating series of interleaving intrusions which carried water across the 'front'. The intrusions were advected upward with the mean flow as they grew in lateral extent, giving the appearance of a spatially developing instability. As they were advected upward, the intrusions passed through the downward propagating phase of the wave modes but they were not substantially reversed, and the compositional layers formed by the intrusions lost any direct relationship with the velocity field of the quasi-horizontal shear layers. While the intrusion thickness, horizontal velocities and formation period were clearly governed by internal wave motions, a theoretical model of the process is needed in order to more precisely understand the nature of the oscillatory process, and this analysis will probably need to include more than one wave mode.

When double-diffusive convection was added, the characteristics of the intrusions were only weakly modified, even when double-diffusive convection was as vigorous as could be achieved (by using a large compositional difference) and the shear layers were made as weak as possible (by using a small forcing buoyancy flux). Convection did, however, cause changes in the vertical density gradient at the intrusion scale that reflected the formation of 'diffusive' density interfaces and salt-fingering layers.

The internal shearing modes transport properties in the horizontal but cannot, on their own, induce a transport of buoyancy. However, in a region of density-compensating horizontal gradients of two components, double-diffusive convection is enhanced by the horizontal displacements in the shear layers, which locally increase vertical gradients favourable to convection, as well as increasing the contact area between water of differing composition. The combination of convection and wave displacements thereby provides efficient horizontal transport of buoyancy. We infer that, where shear layers generate vertical property inversions, they lead to enhanced convection and greater buoyancy fluxes. The convection might be described as parasitic, as it relies on the wave displacements. However, under the conditions achieved in these experiments it does not substantially alter the host wave motions.

Horizontal interleaving intrusions are frequently detected in the ocean thermocline (Fedorov 1978; Ruddick & Richards 2003). The intrusions are characterized by a series of temperature and salinity inversions within a region of mean lateral gradients of temperature and salinity. The growth of such interleaving fine structure at density-compensated T–S fronts has been attributed to double-diffusive fluxes (Ruddick & Richards 2003). On the other hand, inertia–gravity waves of large amplitude are ubiquitous in the ocean thermocline, particularly near the edge of continental shelves and in the Southern Ocean, where it has already been suggested (Georgi 1978) that

internal waves might be responsible for interleaving having lateral extents of order 10 km. Some aspects of the flow in the laboratory experiments (particularly the plume forcing, the finite domain, the upward filling-box advection and shearing modes that are stationary relative to the rigid boundaries) are unlikely to be found in the oceans. However, these elements are merely the artifice by which we maintain in the laboratory a stable stratification, a horizontal gradient region and internal wave activity. The relevant aspect of the laboratory flow is the formation of lateral intrusions at the front by low-frequency internal waves, despite the vertical propagation of the waves through the water column, and irrespective of whether convective fluxes are present. The entrainment flow into the plumes, while primarily only relevant as a mechanism for establishing the background stratification, may also be seen as an ambient extensional flow on either side of the front that begins to affect the stretching of intrusions after they extend far across the front. The two-component experiments demonstrate that once wave displacements initiate interleaving, double-diffusive convection is enhanced throughout volumes very much larger than those that could be reached by the much more slowly growing convectively driven intrusions. It seems likely that under suitable conditions the vertical buoyancy flux due to convection could then take over as the dominant forcing mechanism and continue to drive intrusions initiated by internal waves. Further work is required in order to demonstrate such an evolution, and the effects of a broad spectrum of wave frequencies.

We thank Professors J. S. Turner and G. Veronis for their comments and interest during this work. We also thank T. Beasley for his technical assistance with the experiments. A. A. B. was supported from the Tehran University while on sabbatical leave from the Institute of Geophysics, Tehran University, Iran, in 2003.

REFERENCES

Baines, W. D. & Turner, J. S. 1969 Turbulent buoyant convection from a source in a confined region. *J. Fluid Mech.* **37**, 51–80.

Bidokhti, A. A. 2000 A newly developed low drift fast response salinity meter. *Rev. Sci. Instrum.* **71**, 3539–3542.

Browand, F. K., Guyomar, D. & Yoon, S.-C. 1987 The behavior of a turbulent front in a stratified fluid: Experiments with an oscillating grid. *J. Geophys. Res.* **92**, 5329–5341.

Chen, C. F. 1974 Onset of cellular convection in a salinity gradient due to a lateral temperature gradient. *J. Fluid Mech.* **63**, 563–576.

Chen, C. F. & Chen, F. 1997 Salt-finger convection generated by lateral heating of a solute gradient. *J. Fluid Mech.* **352**, 161–176.

Fedorov, F. N. 1978 *The Thermohaline Finestructure of the Ocean*. (Translated by D. A. Brown, ed. J. S. Turner). Pergamon.

Garrett, C. & Munk, W. 1972 Space-time scales of internal waves. *Geophys. Fluid Dyn.* **2**, 225–264.

Garrett, C. & Munk, W. 1979 Internal waves in the ocean. *Annu. Rev. Fluid Mech.* **11**, 339–369.

Georgi, D. T. 1978 Fine-structure in the antarctic polar front zone: its characteristics and possible relationship to internal waves. *J. Geophys. Res.* **83**, 4579–4588.

Hart, J. E. 1973 Finite amplitude sideways diffusive convection. *J. Fluid Mech.* **59**, 47–64.

Huppert, H. E. & Turner, J. S. 1980 Ice blocks melting into a salinity gradient. *J. Fluid Mech.* **100**, 367–384.

Jeevaraj, C. G. & Imberger, J. 1991 Experimental study of double-diffusive instability in sidewall heating. *J. Fluid Mech.* **222**, 565–586.

Josberger, E. G. & Martin, S. 1981 Convection generated by vertical icewalls. *J. Fluid Mech.* **111**, 439–473.

Malki-Epshtein, L., Phillips, O. M. & Huppert, H. E. 2004 The growth and structure of double-diffusive cells adjacent to a cooled sidewall in a salt-stratified environment. *J. Fluid Mech.* **518**, 347–362.

Maxworthy, T. 1983 Dynamics of double diffusive gravity currents. *J. Fluid Mech.* **128**, 259–282.

Nagasaka, M., Nagashima, H. & Yoshida, J. 1995 Double diffusively induced intrusions into a density gradient. In *Double-Diffusive Convection* (ed. A. Brandt & H. J. S. Fernando). American Geophysical Union.

Narusawa, U. & Suzukawa, Y. 1981 Experimental study of double-diffusive cellular convection due to a uniform lateral heat flux. *J. Fluid Mech.* **113**, 387–405.

Ruddick, B. R. 1985 Momentum transport in thermohaline staircase. *J. Geophys. Res.* **90**, 895–902.

Ruddick, B. R. 2003 Laboratory studies of interleaving. *Prog. Oceanogr.* **56**, 529–547.

Ruddick, B. R., Griffiths, R. W. & Symonds, G. 1989 Stresses across double-diffusive interfaces. *J. Geophys. Res.* **94**, 18161–18173.

Ruddick, B. R., Phillips, O. M. & Turner, J. S. 1999 A laboratory and quantitative model of finite-amplitude thermohaline intrusions. *Dyn. Atmos. Oceans* **30**, 71–99.

Ruddick, B. R. & Richards, K. 2003 Oceanic thermohaline intrusions: observations. *Prog. Oceanogr.* **56**, 499–527.

Ruddick, B. R. & Turner, J. S. 1979 The vertical scale of double-diffusive intrusions. *Deep-Sea Res.* **26A**, 903–913.

Tanny, J. & Tsinober, A. B. 1988 The dynamics and structure of double-diffusive layers in sidewall-heating experiments. *J. Fluid Mech.* **196**, 135–156.

Thorpe, S. A., Hutt, P. K. & Soulsby, R. 1969 The effect of horizontal gradients on thermohaline convection. *J. Fluid Mech.* **38**, 375–400.

Turner, J. S. 1978 Double-diffusive intrusions into a density gradient. *J. Geophys. Res.* **83**, 2887–2901.

Turner, J. S. 1986 Turbulent entrainment the development of the entrainment assumption and its application to geophysical flows. *J. Fluid Mech.* **173**, 431–471.

Turner, J. S. & Chen, C. F. 1974 Two-dimensional effects in double-diffusive convection. *J. Fluid Mech.* **63**, 577–592.

Wells, M. G., Griffiths, R. W. & Turner, J. S. 2001 The generation of density fine-structure by salt fingers in a spatially periodic shear. *J. Geophys. Res.* **106**, 7027–7037.

Wong, A. B. D., Griffiths, R. W. & Hughes, G. O. 2001 Shear layer driven by turbulent plumes. *J. Fluid Mech.* **434**, 209–244.